Theory of the reentrant quantum rotational phase transition in high-pressure HD

Yanier Crespo,[1,2,3] Alessandro Laio,[2,3] Giuseppe E. Santoro,[2,3,1] and Erio Tosatti[2,3,1]

[1]*International Center for Theoretical Physics (ICTP), IT-34014 Trieste, Italy*
[2]*SISSA, Via Bonomea 265, IT-34136 Trieste, Italy*
[3]*Democritos CNR/INFM National Simulation Center, Via Bonomea 265, IT-34136 Trieste, Italy*

The phase diagram of HD near 50 GPa exhibits a reentrant phase transition where a rotationally ordered ("broken symmetry") crystalline phase surprisingly transforms into a rotationally "disordered" high-symmetry phase upon cooling. The qualitative reason for reentrance is the higher entropy of the broken symmetry phase, due to the inequivalence of H and D, as opposed to the low entropy of the high-symmetry phase where the rotational melting is quantum mechanical—a Pomeranchuk-like mechanism. Aiming at a quantitative understanding of this system, we present path integral Monte Carlo (MC) constant-pressure calculations for HD based on empirical but very realistic intermolecular interactions. Ignoring quantum mechanics at first, we use a metadynamics-based classical MC method to seek the lowest-energy zero-temperature classical state, which we identify as a very similar hcp-based structure *C2/c* as hypothesized by Surh *et al.* [Phys. Rev. B **55**, 11330 (1997)]. Upon turning quantum rotational effects on, we calculate the pressure-temperature phase diagram by monitoring a lattice biased order parameter, and find a reentrant phase boundary in good agreement with experiment. The entropy jump across the transition is found to be comparable with $\ln 2$, the value expected for a Pomeranchuk mechanism. A comparison with earlier studies is also presented, yielding relevant information about the role of factors that quantitatively determine the reentrant part of the phase diagram.

I. INTRODUCTION

The molecular hydrogen solids, *para*-H_2, *ortho*-D_2, and HD exhibit very interesting pressure-temperature phase diagrams, where the quantum motion of nuclei dominates at low temperatures. Whereas the molecular centers form in all cases a hexagonal closed-packed (hcp) lattice, the angular molecular orientations undergo a quantum mechanically driven "rotational melting" phase transition, between a high-pressure ordered phase, sometimes called "phase II" or "broken symmetry phase" (BSP),[1–3] and a low-pressure rotationally symmetric phase. In *para*-H_2 and *ortho*-D_2 isolated molecules, only even values of the total angular momentum J are allowed.[4,5] The large rotational kinetic energy gap between the $J = 0$ ground state and the lowest $J = 2$ excited state stabilizes the rotationally melted symmetric phase at low pressures. At large pressures, the crystal field mixes higher rotational states ($J \geqslant 2$) with $J = 0$ in the molecular ground state to an extent that depends on the intermolecular interaction. That interaction, mainly of electric quadrupole-quadrupole (EQQ) origin, favors orthogonal orientations of nearby molecules. As the volume decreases under pressure, symmetry-breaking intermolecular interactions increasingly compete against rotational kinetic energy, eventually overcoming it, and driving the BSP onset at high pressures; at $T = 0$, this is a first-order quantum phase transition. While the phase diagrams for hydrogen and deuterium are qualitatively similar, especially at high temperatures where quantum effects are less important, the low-temperature transition pressure to the BSP phase is much larger in *para*-H_2 ($\approx$110 GPa) than in *ortho*-D_2 ($\approx$28 GPa, see Fig. 1). This mass dependence is a quantum signature, reflecting the lower rotational kinetic energy of D_2 relative to H_2. No accompanying structural change of the lattice formed by molecular centers has been experimentally revealed at these

transitions. Infrared and Raman spectra are compatible with an hcp lattice of molecules persisting from the high-symmetry phase inside the BSP phase for both H_2 and D_2[7,8] apparently excluding a competing face center cubic (fcc) *Pa3* lattice ordering. In solid HD, which is the subject of this study, the same phase transition also takes place. Not surprisingly, it occurs at $\approx$69 GPa, a pressure intermediate between those of hydrogen and deuterium. There is, however, a major difference in HD with respect to H_2 and D_2, a difference that is our present focus. The low-temperature phase diagram of HD exhibits a reentrance, whereby the rotationally ordered ("broken symmetry") crystalline phase somewhat surprisingly reverts back to a rotationally disordered high-symmetry phase upon cooling—apparently the same rotationally melted phase seen at high temperatures. By contrast, in solid *para*-H_2 and *ortho*-D_2, the broken symmetry phase only transforms to a rotationally disordered one upon heating, and there is no reentrance.

The difference between *para*-H_2 or *ortho*-D_2 and HD begins right at the molecular quantum-mechanical level. Since H and D are distinguishable, the lack of inversion symmetry permits all integer values of J, and not just the even ones. As is long known from time honored mean-field approaches,[9–12] a broken-symmetry phase of rotors with all allowed J values and quadrupolar-type interactions has a higher entropy than the rotationally isotropic ("disordered") state,[11] causing a characteristic reentrant shape of the transition line.[9] The underlying physics is easily rationalized at the qualitative level. Since the intermolecular interactions are independent of the isotopic difference between H and D (neglecting the very small dipole moment of HD[13]), the BSP molecular solid phase is made up with HD- or DH-oriented molecules occupying with equal probability each site. This gives rise to an additional entropy of order $\ln 2$ from the two molecular
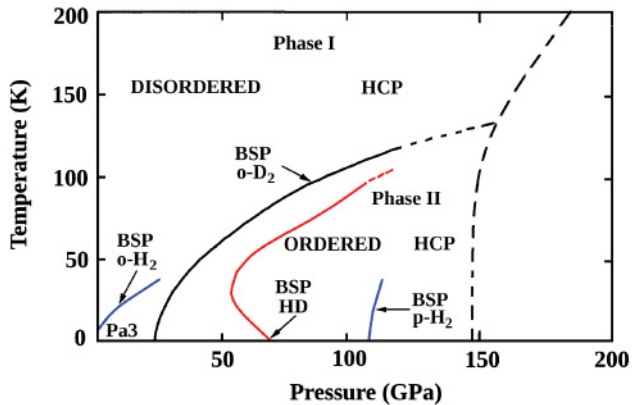
FIG. 1. (Color online) Schematic experimental phase diagram for H2, *ortho*-D$_2$, and HD. Data reported in Ref. [6].

orientations. That entropy term is missing in the quantum rotationally melted state, where the ground state is a single nondegenerate quantum state. The overall situation bears an analogy with the well-known Pomeranchuk effect[14,15] in He^3, the two orientations HD and DH here acting as a pseudospin variable, in place of real nuclear spin in solid He^3.

This simple qualitative picture leaves several important issues still quite open. The main one is a quantitative understanding. A proper theoretical approach, based, for example, on quantum Monte Carlo simulations, should yield an accurate description of the phase diagram, in particular of the reentrant behavior of HD. Important side goals are to clarify the role of different multipole components on the interatomic potential, the role of the lattice structure including the precise nature of the broken symmetry phase, and the difference expected between hcp and fcc ordering of the molecular centers of mass. Other goals to be addressed later will be to clarify the nature of the quantum orientational disorder that sets in below the BSP transition line, and, eventually, to address nucleation phenomena in this unusual regime.

Previous theoretical approaches are mainly based on path-integral Monte Carlo (PIMC), using empirical potentials. Runge *et al.*[16,17] used a potential derived from *ab initio* calculations to address the BSP transition pressure of *ortho*-D$_2$ and assumed an fcc lattice. Using a similar potential, Cui *et al.*[18] described the high-temperature transition lines of *para*-H$_2$ and *ortho*-D$_2$ between BSP and classical rotational disorder in both the fcc and the hcp lattices. The phase diagram of HD was studied in Ref. [19] using PIMC and a potential taking into account only an EQQ interaction of the form given in Ref. [5] [see Eq. (14) and Ref. [20]]. Assuming an fcc lattice, a transition line with a qualitatively correct reentrance was obtained, however, at a pressure of 10 GPa, way below the experimental value.

An important starting element for these studies is a correct BSP crystal structure. Despite many experimental[7,21–26] and *ab initio*[27–30] theoretical studies, that structure is still somewhat uncertain. Some data[26] point to an hcp structure of molecular centers. The anisotropic molecular orientations in the BSP phase are not yet well defined, however, as

experiments do not provide conclusive evidence for a specific structure. The problem of the BSP phase structure has been extensively studied using empirical potentials. Ref. [31] studied the ground-state arrangement of quadrupoles interacting via EQQ interaction on an hcp lattice, concluding that a structure with a space group $Pca2_1$ has the lowest EQQ interaction energy. That configuration was also considered in an *ab initio* calculation using the local density approximation (LDA),[28,32] which suggests that a $Pca2_1$ structure has the lowest energy and wider band gaps. In the end, as in other cases, an accurate empirical modeling of intermolecular interactions offers the best chance to make and to validate the delicate adjustments that comparison with experiment requires.

In this paper, we model the HD solid as an assembly of rigid molecules that have both rotational and translational degrees of freedom, and interact with an empirical potential including isotropic and anisotropic terms. We considered several different potential forms, performing extensive tests in order to select the most appropriate (see Sec. II A). As basic molecular lattices, both hcp and fcc structures are considered and compared. To determine the optimal classical molecular orientations in the BSP range of pressures, we apply a metadynamics-based[33] Monte Carlo search method.[34] The optimal BSP structure obtained in this way has a $C2/c$ symmetry, same as that proposed in Ref. [17] (see Fig. 2). Using this structure as the classical starting point, we study next the low-temperature quantum phase diagram of HD and its reentrant transition line by implementing an accurate PIMC approach. PIMC results place the reentrant phase transition edge at a pressure of $\approx$56 GPa and a temperature of $\approx$ 25 K in good agreement with the experimental values of $\approx$53 GPa and $\approx$30 K. Comparison with results obtained with slightly different potentials, with increasing Trotter numbers and frozen versus deformable underlying lattice structures, sheds light on the influence of these different ingredients in determining the experimental reentrance and its features.

II. THEORY

A. The Hamiltonian of the system

We aim at describing a hydrogen-like molecular solid in a regime of pressures where the molecules are still well-defined objects moderately interacting among each other, via an intermolecular potential $\hat{U}$. That potential can be seen as the Born-Oppenheimer total energy of electrons plus nuclei as a function of all molecular coordinates. In principle, accessible through *ab initio* electronic calculations, the total energy would at the same be computationally expensive and difficult to translate in our desired pairwise form, $\hat{U} = \sum_{i<j} U_{ij}^{\text{pair}}$. Good semiempirical pairwise forms of $\hat{U}$ have been adopted, some tested against LDA *ab initio* simulations,[16–18] and we will follow suit. We neglect the vibrational degree of freedom within each molecule, and consider each molecule as a rigid rotor with a center of mass (CM) at the position $\mathbf{R}_{\text{CM}_i}$ and orientation $\mathbf{\Omega}_i = (\theta_i, \phi_i)$, with (θ_i, ϕ_i) the inclination and azimuthal angles in spherical coordinates. The molecules
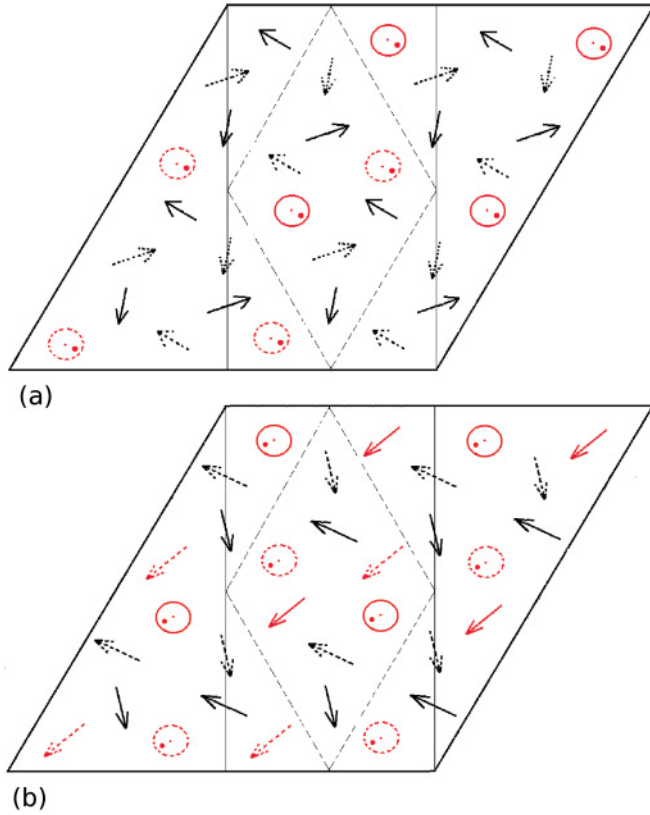
FIG. 2. (Color online) The new structure having the lowest classical energy as seen along the HCP axis. The primitive cell has a diamond shape (dashed line) and contains 16 molecules. The cell consist of two layers AB and $A'B'$. Molecules in the upper layers (B, B') are shown in solid line, while the lower layer is shown with dashed line. The AB layers (a) lie above the $A'B'$ layers (b). This structure belongs to the space group $C2/c$.

have therefore just translational and rotational degrees of freedom, and the Hamiltonian is a sum of kinetic and potential terms:

$$\hat{H} = \hat{K} + \hat{U}(\{\mathbf{R}_{\mathrm{CM}_i}, \mathbf{\Omega}_i\}), \tag{1}$$

$$\hat{K} = K^{\mathrm{tra}} + K^{\mathrm{rot}} = -\lambda \sum_{i=1}^{N} \hat{\nabla}_{\mathbf{R}_{\mathrm{CM}_i}}^2 + B \sum_{i=1}^{N} \hat{L}_i^2, \tag{2}$$

where N is the number of molecules, $\lambda = \frac{\hbar^2}{2M_T}$ with M_T is the total mass of the molecule, $B = \frac{\hbar^2}{2I}$ is the rotational constant with I the molecular moment of inertia, $\hat{\nabla}^2$ is the Laplacian, and $\hat{L}$ is the angular momentum operator. Quantum effects appear through the relatively large values of λ and B. The effect of quantum statistics is, in principle, twofold (i) intramolecular, where the statistics governs the allowed values of the angular momentum operator $\hat{L}$, and (ii) intermolecular, with all molecules being identical indistinguishable and interchangeable. We include and treat in full the effects (i), whereas we neglect the effect (ii), since intermolecular exchanges are totally unimportant at the regimes of pressure and temperatures we are interested in. The pairwise interaction

potential is expanded in spherical harmonics

$$
\begin{aligned}
&U^{\mathrm{pair}}(\mathbf{\Omega}_1, \mathbf{\Omega}_2, \mathbf{R}_{12}) \\
&= (4\pi)^{3/2} \sum_{l_1, l_2, l} B_{l_1 l_2 l}(R_{12}) \sum_{m_1, m_2, m} (l_1, m_1, l_2, m_2 | l_1, l_2, l, m) \\
&\quad \times Y_{l_1, m_1}(\mathbf{\Omega}_1) Y_{l_2, m_2}(\mathbf{\Omega}_2) Y_{l, m}^*(\hat{\mathbf{\Omega}}_{12})
\end{aligned}
$$

where $(l_1, m_1, l_2, m_2 | l_1, l_2, l, m)$ are Clebsch-Gordan coefficients,[5] $\mathbf{R}_{12}$ is the vector connecting the geometric center points of two molecules (which can be easily calculated in terms of $\mathbf{R}_{\mathrm{CM}_{1,2}}$ and $\mathbf{\Omega}_{1,2}$), the sum being restricted to even values of l_1 and l_2. By far, the dominant contribution at low pressures (large R_{12}) is the isotropic component associated to $l_1 = l_2 = l = 0$. Next in importance is the EQQ interaction, $l_1 = 2$, $l_2 = 2$, $l = 4$ and the atom-diatom terms[20] $l_1 = 2$, $l_2 = 0$, $l = 2$ and $l_1 = 0$, $l_2 = 2$, $l = 2$ whose radial part ($B_{l_1, l_2, l}$) becomes more important than the EQQ interaction at high pressure. The atom-diatom terms cancel out exactly on an ideal fcc or hcp lattices because of symmetry. Therefore in a finite but low-temperature configuration, their values will be small, compared with the EQQ interaction. Finally, nonnegligible at closer distances are terms with $l_1 = l_2 = 2$, $l = 0$ and $l_1 = l_2 = 2$, $l = 2$. In summary, in the range of pressure of interest, 0–100 GPa, the EQQ interaction is the leading contribution. The associated coefficients $B_{l_1 l_2 l}(R_{12})$ have been extensively studied, for instance, by Schaefer et al.[35] and by Burton et al.[36] (see also Refs. 37–39).

Following a well established practice, we construct the interaction potential in the solid phase, by an appropriate rescaling of the gas-phase ingredients. The resulting hybrid potential is essentially that of Cui et al.,[18]

$$U_{\mathrm{pot}} = \sum_{i<j} U_{\mathrm{iso}}(R_{ij}) + \eta \sum_{i<j} U_{\mathrm{ani}}^{\mathrm{pair}}(\mathbf{\Omega}_i, \mathbf{\Omega}_j, \mathbf{R}_{ij}). \tag{3}$$

Here, the isotropic component U_{iso} (related to B_{000}) is tailored so as to lead to a good agreement with the known equation of state (EOS) of both H_2 and D_2:[40]

$$
\begin{aligned}
P = 3K_0 \left(\frac{V}{V_0}\right)^{-\frac{2}{3}} &\left[1 - \left(\frac{V}{V_0}\right)^{\frac{1}{3}}\right] \\
&\times \exp\left\{\frac{3}{2}(K_0' - 1)\left[1 - \left(\frac{V}{V_0}\right)^{\frac{1}{3}}\right]\right\},
\end{aligned} \tag{4}
$$

(V_0 is the volume at zero pressure, and $K_0 = 0.252\,79$ and $K_0' = 7.0642$ are calculated by fitting Eq. (4) to the results obtained from the simulation of an HD system using the constant pressure PIMC technique, see Sec. II C); the anisotropic terms are included by rescaling the sum of two-body gas-phase interactions with a parameter $\eta \approx 0.61 + 0.31(R_{\mathrm{nn}}/R_{\mathrm{nn}}^0 - 0.5)$ (R_{nn}^0 and R_{nn} being the nearest-neighbor distances at zero pressure and at pressure P, respectively) determined by Runge et al.[16,17] through a fitting of LDA data. The sum over i and j is cut off at next-nearest neighbors. We refer the reader to Refs. 16–18 and 35 for the details of $U_{\mathrm{iso}}(R_{ij})$ and $U_{\mathrm{ani}}^{\mathrm{pair}}(\mathbf{\Omega}_i, \mathbf{\Omega}_j, \mathbf{R}_{ij})$. We consider here two sources for the coefficients $B_{l_1 l_2 l}(R_{12})$ appearing in $U_{\mathrm{ani}}^{\mathrm{pair}}$: first Schaefer et al.[35] which we denote by $U_{\mathrm{Cui}}^{\mathrm{Schaefer}}$; second, Burton et al.[36] denoted by $U_{\mathrm{Cui}}^{\mathrm{Burton}}$. Remarkably, these two choices

lead to approximately the same EOS, but show a considerable difference in the BSP transition pressure, see Sec. III.

B. Path-integral representation of rotors

The path-integral Monte Carlo approach to the quantum rotor model in Eq. (1) is quite standard, and we refer the reader to Ref. 18 for details. The PIMC method allows to obtain a numerical solution of the many-body problem represented by the Hamiltonian (1) at finite temperatures. The density matrix $e^{-\beta \hat{H}}$, where $\beta = 1/k_B T$, fully describes the quantum-statistical properties of the system at finite temperature T. In the position basis, the density matrix has the form:

$$\rho(\mathbf{X}', \mathbf{X}, \beta) = \langle \mathbf{X}' | \underbrace{e^{-\tau \hat{H}} \cdots e^{-\tau \hat{H}}}_{Q \text{ times}} | \mathbf{X} \rangle,$$

where $\tau = \beta/Q$ is the time step, the integer Q is the number of Trotter slices,[41] and we use the shorthand notation $\mathbf{X} = \mathbf{R}_{\mathrm{CM}_1}, \mathbf{\Omega}_1, \ldots, \mathbf{R}_{\mathrm{CM}_N}, \mathbf{\Omega}_N$. The partition function $Z = \mathrm{Tr}\{e^{-\beta \hat{H}}\}$ can be calculated as an integral of the diagonal component of ρ:

$$Z = \Delta d\mathbf{X}_0 \rho(\mathbf{X}_0; \mathbf{X}_0, \beta). \tag{5}$$

Inserting a complete set of states between each exponential, we obtain

$$\rho(\mathbf{X}'; \mathbf{X}, \beta) = \Delta d\mathbf{X}_1 \cdots d\mathbf{X}_{Q-1} \rho_{\mathbf{X}_0, \mathbf{X}_1} \cdots \rho_{\mathbf{X}_{Q-1}, \mathbf{X}_Q}, \tag{6}$$

where we have defined $\rho_{\mathbf{X}_{q-1}, \mathbf{X}_q} = \rho(\mathbf{X}_{q-1}, \mathbf{X}_q, \tau)$, with $\mathbf{X}_0 = \mathbf{X}, \mathbf{X}_Q = \mathbf{X}'$, and $\mathbf{X}_q = \{\mathbf{R}_{\mathrm{CM}_{1,q}}, \mathbf{\Omega}_{1,q}, \ldots, \mathbf{R}_{\mathrm{CM}_{N,q}}, \mathbf{\Omega}_{N,q}\}$. For τ small enough, we can approximate the density matrix operator using the primitive approximation:[41]

$$e^{-\tau(\hat{K} + \hat{U})} \approx e^{-\tau \hat{K}} e^{-\tau \hat{U}}. \tag{7}$$

For the Hamiltonian (1), the density matrix, in the primitive approximation, can be written explicitly:

$$\rho_{\mathbf{X}_{q-1}, \mathbf{X}_q} = [4\pi \tau \lambda]^{-\frac{3N}{2}} e^{\left[-\sum_{i=1}^{N} \frac{(\mathbf{R}_{\mathrm{CM}_{i,q-1}} - \mathbf{R}_{\mathrm{CM}_{i,q}})^2}{4\tau \lambda} \right]}$$

$$\times \prod_{i=1}^{N} \left[\sum_{l=0}^{\infty} \frac{2l+1}{4\pi} P_l\big(\cos(\Theta_{i,q})\big) e^{-\tau B l(l+1)} \right]$$

$$\times e^{\left\{ -\frac{\tau}{2} [U(\mathbf{X}_{q-1}) + U(\mathbf{X}_q)] \right\}}, \tag{8}$$

where $\cos(\Theta_{i,q}) = \mathbf{n}_{i,q-1} \cdot \mathbf{n}_{i,q}$, with $\mathbf{n}_{i,q} = [\cos(\phi_{i,q}) \sin(\theta_{i,q}), \sin(\phi_{i,q}) \sin(\theta_{i,q}), \cos(\theta_{i,q})]$, and $P_l(\bullet)$ are Legendre polynomials.

C. Constant-pressure ensemble

An advantage of the Monte Carlo (MC) method is that it can be readily adapted to the calculation of averages in any ensemble. As we are interested in studying the temperature versus the pressure phase diagram of HD, most calculations were performed in the constant-pressure ensemble, where the number of molecules N, the pressure P, and the temperature T are constant. In this ensemble, the partition function

is given by

$$Z_{\mathrm{NPT}} = \Delta d\mathrm{V} \Delta d\overline{\mathbf{X}} \ \mathrm{V}^{NQ} e^{-\beta \mathrm{PV}} \rho(\overline{\mathbf{X}}; \overline{\mathbf{X}}, \beta), \tag{9}$$

where V is the volume of the simulation cell. Note that in this equation we used a set of scaled coordinates $\overline{\mathbf{X}} = \{\overline{\mathbf{R}}_{\mathrm{CM}_{i=1,\ldots,N, q=1,\ldots,Q}}, \mathbf{\Omega}_{i=1,\ldots,N, q=1,\ldots,Q}\}$, where $\overline{\mathbf{R}}_{\mathrm{CM}_{i,q}} = L_{\mathrm{Box}}^{-1} \mathbf{R}_{\mathrm{CM}_{i,q}}$. In this case, the configurational integral in Eq. (9) extends over the unit cube[42] and the additional factor V^{NQ} comes precisely from the volume element $d\mathbf{X} = V^{NQ} d\overline{\mathbf{X}}$. The Metropolis scheme is implemented by generating a Markov chain[41] of states, which has a limiting distribution proportional to

$$\exp\left\{ -\beta \left[PV - \frac{NQ}{\beta} \ln(V) \right] \right\} \rho(\overline{\mathbf{X}}; \overline{\mathbf{X}}, \beta). \tag{10}$$

A new state is generated by displacing a molecule randomly and/or by making a random volume change. One important difference between this ensemble and the canonical ensemble is that when a move involves a change in volume, the density of the solid changes. In this case, the potential energies in the initial and final states are different and must be recalculated from scratch, which is computationally more expensive than changing the configuration by moving just one molecule.

As we are working in the rigid-rotor approximation, the intramolecular distance must not change during a volume move. This implies the constraint $\mathbf{r}'_{2i,q} - \mathbf{r}'_{1i,q} = \mathbf{r}_{2i,q} - \mathbf{r}_{1i,q}$, to be satisfied by the coordinates of atoms 1 and 2 in the same molecule. To satisfy that, we change the atoms positions according to

$$\mathbf{r}'_{1i,q} = \left(\frac{L'_{\mathrm{Box}}}{L_{\mathrm{Box}}} - 1 \right) \mathbf{R}_{\mathrm{CM}_{i_q}} + \mathbf{r}_{1i,q},$$

$$\mathbf{r}'_{2i,q} = \left(\frac{L'_{\mathrm{Box}}}{L_{\mathrm{Box}}} - 1 \right) \mathbf{R}_{\mathrm{CM}_{i_q}} + \mathbf{r}_{2i,q}.$$

III. RESULTS

A. Classical orientational order of hydrogen molecules on the hcp lattice

In order to determine the BSP-isotropic coexistence line of HD, it is necessary to establish first of all the BSP molecular crystal structure at the classical level. If the molecular centers form an hcp lattice, we need to establish the optimal geometry of molecular orientations, and an appropriate order parameter to measure and monitor that angular order. Suppose we know the structure of the ordered phase; then we can define N unit vectors $\mathbf{u}_i$ corresponding to the orientation of molecule on all sites $i = 1, N$. Thus, following Runge et al.,[16] we define the order parameter

$$O_p = \left\{ \sum_{q=1}^{Q} \sum_{i=1}^{N} \frac{1}{2QN} [3\cos^2(\mathbf{n}_{i,q} \cdot \mathbf{u}_i) - 1] \right\}^2, \tag{11}$$

where, as before, $\mathbf{n}_{i,q}$ labels the orientation of the molecule i in the Trotter slice q for a given configuration visited with the PIMC algorithm. This order-parameter measures the extent of ordering (and by difference, its deviation) relative to a given orientational structure defined by the set $\{\mathbf{u}_i\}$. In Ref. 16, the set $\{\mathbf{u}_i\}$ was selected as the four (111) directions of *Pa3* on the fcc lattice, *Pa3* being the lowest potential energy state of the EQQ interaction on the fcc lattice. In the perfect ordered state of *Pa3*, $\langle O_p \rangle = 1$, while disorder is signaled by $\langle O_p \rangle \approx 0$. If, however, solid HD, in the orientational disordered phase, has an hcp lattice,[43] it is necessary to define a different set of vectors $\{\mathbf{u}_i\}$, corresponding to the BSP low-energy classical structure, to be used in Eq. (11).

To find the most likely BSP structure, which minimizes the potential energy on an hcp lattice, we implement the classical metadynamics-based MC method proposed in Ref. 34 in a system of 216 classical molecules whose charge center is fixed onto an hcp lattice at $T = 20$ K. The metadynamics simulation uses as a collective variable the potential energy $s = U_{\text{pot}}$ [see Eq. (3)]. The history-dependent potential is mapped onto a grid with a spacing of 1×10^{-5} a.u., using Gaussians of height 1×10^{-4} a.u.

We performed several independent runs with the same set of parameters, always starting from the configuration with the lowest energy obtained in the previous run. In Fig. 2, we show the structure of minimum energy found in this manner. The diamond-shaped primitive cell (dashed line) contains 16 molecules. This cell consists of two pairs of layers, AB and $A'B'$. Molecules in the upper layers (B, B') are shown as solid, while those in the lower layers are shown as dashed. The AB layers (a) lie above the $A'B'$ layers (b). The arrows in Fig. 2 are pointing toward the positive direction of the HCP axis. The lattice parameters and the atomic coordinates of the optimized structure are given in Appendix, Table I. This structure is monoclinic and belongs to the same space group $C2/c$, same symmetry as that proposed as the quantum ground state of H_2 on the HCP lattice by Surh *et al.*[17] The potential energy of the new structure is ≈ 54 meV lower than that of a structure obtained by optimizing the molecular orientations starting from a guess similar to that of Ref. 17.

The order parameter in Eq. (11) suffers from an important limitation, namely, if the system reaches an ordered structure different from the reference one associated to the chosen set $\{\mathbf{u}_i\}$, still $O_p \approx 0$. Thus the condition $O_p = 0$ is not sufficient to ensure that the system is in an orientationally disordered phase. To address this issue further, we monitored a second order parameter defined as

$$\langle O_Q \rangle = \frac{1}{N} \sum_{i=1}^{N} \frac{1}{6} \sum_{j,k=1}^{3} \left(\mathcal{Q}_{jk}^{\text{Total}} \right)^2, \quad (12)$$

where

$$\mathcal{Q}_{jk}^{\text{Total}} = \frac{1}{T_{\text{MC}} Q} \sum_{a=1}^{2 T_{\text{MC}} Q} \left(3 r_{j,a}^i r_{k,a}^i - r_0^2 \delta_{jk} \right) \quad (13)$$

with T_{MC} the MC time. $\mathcal{Q}_{jk}^{\text{Total}}$ is the quadrupolar moment of a system of $T_{\text{MC}} Q$ molecules with a charge per atom of $(T_{\text{MC}} Q)^{-1}$. If the molecules rotate in MC or Trotter time (showing spherical symmetry), then $\mathcal{Q}_{jk}^{\text{Total}} = 0$; if, on the contrary, the molecules are frozen in a quadrupolar configuration both in MC and Trotter time, then $\frac{1}{6} \sum_{j,k=1}^{3} (\mathcal{Q}_{jk}^{\text{Total}})^2 = 1$. Thus $\langle O_Q \rangle$ signals quadrupolar order in a more general way than $\langle O_p \rangle$, which is restricted to a particular choice of $\{\mathbf{u}_i\}$. We checked nonetheless that both parameters give essentially the same transition pressure, indicating that the orientational order of the phase in Fig. 2 is likely to be thermodynamically favored in the range of pressure and temperature considered here.

B. The transition line from rotationally spherical to the BSP state

We carried out several simulations aimed at computing the BSP transition line of solid HD. A transition is detected by monitoring the value of the order parameter in Eq. (11) as a function of MC time. Consider, for example, a constant pressure PIMC (CP-PIMC) for a system of 64 molecules of HD on an HCP lattice, with a time-step of $\tau = 4.55 \times 10^{-2} B^{-1}$ using the $U_{\text{Cui}}^{\text{Burton}}$ interaction potential. The inset of Fig. 3 shows the order parameter as a function of MC time at four pressures: 52 GPa (open circles), 54 GPa (open squares), 56 GPa (solid diamond), and 58 GPa (solid up triangles). For $P < 56$ GPa, after an initial transient, $\langle O_p \rangle$ converges to a small value $\langle O_p \rangle \approx 0$, while for $P = 58$ GPa $\langle O_p \rangle$ shows an upward turn and converges to a nonzero value $\langle O_p \rangle \approx 0.3$. This abrupt
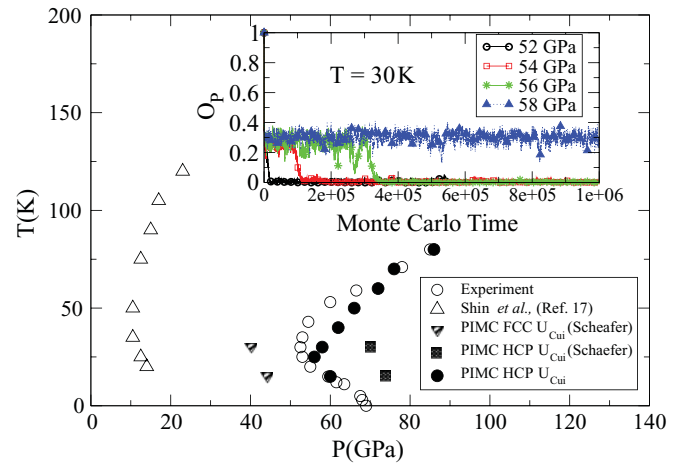
FIG. 3. (Color online) The temperature-pressure phase diagram of solid HD. The open circles are the experimental data.[3] The up open triangles are the CV-PIMC results reported by Shin *et al.*[19] The down triangles are CP-PIMC results considering the system of Fig. 4 using the $U_{\text{Cui}}^{\text{Schaefer}}$ potential. The solid squares and solid circles are CP-PIMC results for a system of 64 molecules of HD on an HCP lattice and a time step of $\tau = 4.55 \times 10^{-2} B^{-1}$ using $U_{\text{Cui}}^{\text{Schaefer}}$ and $U_{\text{Cui}}^{\text{Burton}}$, respectively. Inset: lattice biased order parameter as a function of the MC time for four pressures: 52 GPa (open circles), 54 GPa (open squares), 56 GPa (solid diamond), and 58 GPa (solid up triangles).

change in the order parameter indicates the presence of a phase transition from a disordered phase to an ordered one, suggesting that HD, at a temperature of $T = 30$ K, orders at ≈ 58 GPa. We carried out several checks aimed at assessing the robustness of our results with respect to the simulation details. In particular, we found that (i) the Hamiltonian in Eq. (1) requires that translations and rotations are related to the centers of mass of the molecules, while the intermolecular potential needs to be calculated starting from the geometric centers of the molecules.[5] If one theoretically wanted to nail down the molecules in some fixed lattice, accounting only for rotational degrees of freedom, the question arises of which centers to keep fixed: centers of mass, or geometric centers? We have addressed this point and found that if in Eq. (1) one neglects the translational degrees of freedom and assumes that the molecules just rotate around the center of mass, the transition pressure decrease drastically and unrealistically to a few GPa. The transition becomes crossover-like where the order parameter increases slowly and smoothly with pressure, and the re-entrance becomes imperceptible. We suppose that the reason for this behavior is the symmetry of the interaction potential with respect to the geometrical center. This discourages motion, keeping the center of mass fixed, strongly favoring the ordered phase. (Indeed, an expansion of the pairwise interaction around the centers of mass of the two molecules would involve extra contributions, which have been discussed in Ref. 44.) Therefore, assuming fixed centers of mass appears to be a poor choice, and geometrical centers, which in HD differ from the centers of mass of the molecules, should make a better one. To test this conjecture, we performed simulations in which the geometrical centers are now held fixed in an hcp lattice. This system has a transition pressure very close to the one obtained allowing translations. The same behavior can be observed in the case of H_2 and D_2 (e.g., compare the results of Refs. 18 and 16). The conclusion is that once the symmetry of the interaction of rotors is properly centered at the geometrical centers, and not at the molecular centers of mass, then it is relatively unimportant to allow for translational degrees of freedom. (ii) The number of replicas does not change significantly the transition pressure, and changing that number just makes it fluctuate in a small range. We get a transition pressure of 56 GPa for $\tau = 0.2 B^{-1}$, 60 GPa for $\tau = 6.83 \times 10^{-2} B^{-1}$, and 58 GPa for $\tau = 4.55 \times 10^{-2} B^{-1}$ for a CP-PIMC calculation at $T = 30$ K for 64 molecules. (iii) The transition pressure only gently decreases as the system size is increased. We get a transition pressure of 56 GPa for 64 molecules, 54 GPa for 128 molecules, and 54 GPa for 256 molecules, for a CP-PIMC calculation at $T = 30$ K and $\tau = 0.2 B^{-1}$.

With the protocol described above, we then repeated the procedure shown in the inset of Fig. 3 for several choices of T, the interaction potential, and lattice. This allowed estimating approximately the transition pressure as a function of T.

Figure 3 shows the temperature-pressure phase diagram of solid HD, along with the experimental transition line (open circles, from Ref. 3), also compared to theoretical phase diagrams obtained in previous calculations. The up open triangles are the constant volume PIMC (CV-PIMC) results reported by Shin *et al.*[19] The down triangles are CP-PIMC results considering
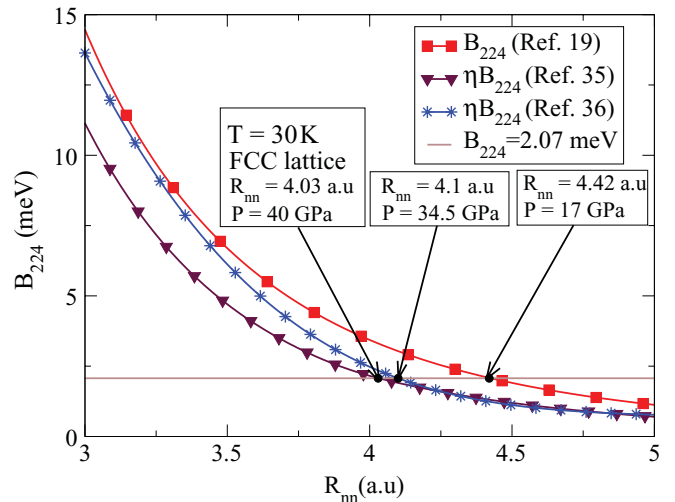
FIG. 4. (Color online) EQQ interaction term of the intermolecular potential as a function of the nearest-neighbor distance from three sources. Solid squares: EQQ interaction used in Ref. 19, solid down triangles and stars are the scaled EQQ interaction using the data reported in Refs. 35 and 36, respectively, and the scale factor of Ref. 16. The data shown are results from CV-PIMC simulation on a system consisting of 108 molecules of HD fixed on a fcc lattice at $T = 30$ K and a time step of $\tau = 6.83 \times 10^{-2} B^{-1}$. The pressure was calculated using the Vinet *et al.*[40] equation of state with the fitting parameters $K_0 = 0.252\,79$, $K_0' = 7.0642$ obtained with our CP-PIMC simulation.

the system of Fig. 4 using the $U_{\text{Cui}}^{\text{Schaefer}}$ potential. The solid squares and solid circles are CP-PIMC results for a system consisting of 64 molecules of HD on an hcp lattice using $U_{\text{Cui}}^{\text{Schaefer}}$ and $U_{\text{Cui}}^{\text{Burton}}$, respectively (the time step used was $\tau = 4.55 \times 10^{-2} B^{-1}$).

We obtain a reentrant behavior for the HD phase line on both the realistic hcp and the fictitious fcc lattices, and for both choices of potentials ($U_{\text{Cui}}^{\text{Schaefer}}$ and $U_{\text{Cui}}^{\text{Burton}}$). The reentrant phase line edge point—the minimum pressure P_e at which the transition occurs—is $P_e \approx 56$ GPa for the hcp lattice with the $U_{\text{Cui}}^{\text{Burton}}$ potential, close to the experimental value of $P_e = 53$ GPa and in much better agreement than the previous PIMC calculations reported in Ref. 19, which give $P_e \approx 10$ GPa. Using alternatively $U_{\text{Cui}}^{\text{Schaefer}}$ yields instead $P_e \approx 70$ GPa. The edge point temperature $T_e = 25$ K is also in good agreement with the experimental value of $T_e = 30$ K. In general, the BSP line obtained with the $U_{\text{Cui}}^{\text{Burton}}$ potential is in fairly good agreement with the experiment. Interestingly, the BSP transition line for the fcc lattice is strongly shifted downward by about 30 GPa, regardless of the potential used. In that case, the BSP structure is *Pa3*, and the stronger tendency to order is evidently due to the lack of frustration in fcc. In other words, it is the angular frustration present in the hcp lattice, and the connected poorer relative stability of the *C2/c* structure that renders the BSP angular structure much more prone to melting than the *Pa3*.

It is interesting to analyze the reentrant phase line just obtained using thermodynamics. The inverse slope of that line is, according to Clapeyron's equation, $dP/dT = \Delta S/\Delta V$,

directly connected to the entropy jump ΔS between the low-temperature quantum rotationally melted phase and the higher-temperature BSP solid phase. Even though the transition is always first order, the inverse slope and the entropy jump vanish both at $T = 0$ (where due to Nernst's theorem entropy vanishes in both phases) and at the reentrant edge point (where both entropies are finite, and just happen to coincide). In between, the entropy jump is finite, from the slope, we estimate a maximum value $\Delta S \sim 0.4k_B \pm 0.2$ near 60 GPa at 15 K, to be compared with $0.5k_B$ of the experimental slope at same pressure and temperature (see Fig. 3). In a Pomeranchuk-type reentrance, the entropy jump should be comparable to, although smaller than, $\ln 2 = 0.693$; and that is indeed the case here. The physical interpretation of this result is that indeed the BSP phase has an entropy close to $\ln 2$ due to the (HD, DH) disorder at each site, whereas the low-temperature, quantum rotationally melted phase can at most have an activated entropy $\sim \exp{-\Delta/k_B T}$, where Δ is the gap above the nondegenerate ground state. The two (HD, DH) distinguishable orientations therefore act as a kind of pseudospin doublet, raising the entropy of the solid, apparently more ordered BSP phase, above that of the apparently less ordered symmetric phase. The reentrant transition of HD therefore represents, in Frenkel's language, another "entropy-driven phase transition."[45]

The systematic study that we did of the behavior of various potentials permits an assessment of the sensitivity of the BSP transition line to the parameters of the problem. Besides the entropy terms just mentioned, the BSP transition occurs from a balance between the rotational kinetic energy (lowest in the symmetric phase) and EQQ interaction energy (lowest in the BSP phase). Consider the EQQ interaction term of the intermolecular potential as a function of the nearest-neighbor distance for a fixed configuration of the molecules. This quantity is plotted in Fig. 4 as a function of the nearest-neighbor distance R_{nn}. The three different choices of B_{224} shown are associated to (i) the $1/R_{nn}^5$ pure EQQ choice

$$B_{224}(R_{nn}) = \frac{\Gamma_0 (R_{nn}^0)^5}{(4\pi)^{3/2}} \left(\frac{1}{R_{nn}} \right)^5 \qquad (14)$$

of Ref. 19 (solid squares), where $\Gamma_0 = 117.7$ K[20], (ii) the choice of Ref. 35 rescaled with the factor $\eta \approx 0.61 + 0.31(R_{nn}/R_{nn}^0 - 0.5)$ (solid down triangles), and (iii) the choice of Ref. 36 rescaled with the same factor η (stars). If we consider, for illustration purposes, a horizontal cut of the interaction energy term B_{224} with a fixed value of 2.07 meV (horizontal line in Fig. 4), which we found to be appropriate to describe the transition in fcc at $T = 30$ K. The various choices of B_{224} attain this fixed value at different R_{nn} (see the three boxes in Fig. 4), which we can convert from volume to pressure by the equation of state of Vinet *et al.*[40] in Eq. (4) (for this purpose we used the fitting parameters $K_0 = 0.252\,79$, $K_0' = 7.0642$ obtained with our CP-PIMC simulations). Remarkably, three different CV-PIMC simulations (with a time step of $\tau = 6.83 \times 10^{-2} B^{-1}$) of a system of 108 HD molecules on a fcc lattice at $T = 30$ K, with

the three choices of B_{224} illustrated in Fig. 4 lead to a value of the transition pressure quite close to the values predicted by the cut at 2.07 meV. A similar systematic agreement is observed in all the other cases studied, showing the crucial role played by the choice of the EQQ interaction in determining the BSP transition pressure; a EQQ interaction shifted toward larger values of R_{nn} is associated to a larger transition volume and hence a smaller transition pressure, via the EOS in Eq. (4).

In summary, we have applied PIMC within both the constant-volume and constant-pressure ensembles to the reentrant phase diagram of the HD solid at high pressures and low temperatures, considering both hcp (realistic) and fcc (fictitious) lattices. We studied the influence of the potential chosen, the translational degrees of freedom, and the choice of the EQQ interaction potential on the BSP transition line. It was found that while the translational degrees of freedom have a small effect on the transition pressure (see Sec. III B), the choice of lattice and interaction potential strongly affects the transition pressure. Using a metadynamics-based MC scheme, we found that a $C2/c$ ordered structure, containing 16 molecules per cell is, with the best available potentials, energetically preferred for the classical BSP phase on an hcp lattice. Successive implementation of quantum molecular rotations by path-integral Monte Carlo permitted a full calculation of the reentrant BSP-rotationally symmetric phase line. The transition was identified using two order parameters, one dependent on the new structure and the second related to the total quadrupolar moment of the molecule, particularly sensitive to the rotational state of the molecule. The phase line was calculated for both the hcp and the fcc lattices, yielding a realistic reentrant behavior in both cases.

The best results are obtained with the $U_{\text{Cui}}^{\text{Burton}}$ potential on the hcp lattice, with features of the BSP-symmetric coexistence line in good agreement with experiment. The orientationally ordered state edge was found at a minimum pressure $P_e \approx 56$ GPa for the hcp lattice and the Cui-Burton potential, quite close to the experimental value $P_e = 53$ GPa and in much better agreement than the previous PIMC calculations reported in Ref. 19, which gave $P_e = 10$ GPa. The edge point temperature $T_e = 25$ K is also in good agreement with the experimental one $T_e = 30$ K. Finally, the entropy jump at the phase transition is found to have a maximum value below but not far from $\ln 2$, in agreement with a Pomeranchuk-like, entropy-driven picture of the reentrant transition. Further work to investigate in more detail phenomena such as nucleation connected with this quantum-classical transition is being planned for the future.

APPENDIX: THE OPTIMAL *C2/c* STRUCTURE

We report here the atomic coordinates for the optimized *C2/c* structure we have found.

TABLE I. Lattice parameters and atomic coordinates for the optimized *C2/c* structure shown in Fig. 2. β is the angle between the *a* and *c* axes.

Lattice parameters											
$b/a = 0.577\,235$				$c/a = 1.373\,826$				$\beta = 136.7102°$			
Atomic coordinates in units of *a*											
	x	y	z		x	y	z		x	y	z
H1	0.45206	0.435922	0.104149	H23	0.69003	0.547808	0.122962	H44	−0.599541	0.174267	0.572134
H2	0.38144	0.429931	0.131383	H24	0.64343	0.0296006	0.112562	H45	−0.17294	0.279394	0.389543
H3	−0.432991	0.402939	0.80761	H25	−0.0479407	0.141313	0.575158	H46	−0.16049	0.297669	0.316923
H4	−0.400461	0.462885	0.840892	H26	−0.118561	0.147305	0.602392	H47	−0.309971	0.318045	0.59397
H5	0.17294	0.568011	0.0814657	H27	0.0670096	0.174296	0.336602	H48	−0.356571	0.259017	0.58357
H6	0.16049	0.00905105	0.154086	H28	0.0995396	0.11435	0.369883	H49	0.047939	0.429931	0.837868
H7	−0.690031	0.0294275	0.819056	H29	−0.327061	0.00922422	0.552474	H50	0.118559	0.435922	0.810634
H8	−0.643431	0.547635	0.829456	H30	−0.339511	0.568184	0.625094	H51	−0.0670102	0.462914	0.134407
H9	0.0479396	0.435922	0.366859	H31	−0.19003	0.547808	0.348047	H52	−0.0995401	0.402968	0.101126
H10	0.11856	0.429931	0.339625	H32	−0.14343	0.0296006	0.358447	H53	−0.672941	0.297842	0.860552
H11	−0.0670107	0.402939	0.605416	H33	−0.0479401	0.147305	0.104149	H54	−0.660491	0.279567	0.787932
H12	−0.0995407	0.462885	0.572134	H34	−0.11856	0.141313	0.131383	H55	0.19003	0.25919	0.122962
H13	0.32706	0.568011	0.389543	H35	0.0670091	0.114321	0.80761	H56	0.14343	0.318218	0.112562
H14	0.33951	0.00905105	0.316923	H36	0.099539	0.174267	0.840892	H57	−0.547941	0.429931	0.575158
H15	0.190029	0.0294275	0.59397	H37	0.67294	0.279394	0.0814657	H58	−0.618561	0.435922	0.602392
H16	0.143429	0.547635	0.58357	H38	0.66049	0.297669	0.154086	H59	0.56701	0.462914	0.336602
H17	−0.452061	0.141313	0.837868	H39	−0.190031	0.318045	0.819056	H60	0.59954	0.402968	0.369883
H18	−0.381441	0.147305	0.810634	H40	−0.143431	0.259017	0.829456	H61	0.172939	0.297842	0.552474
H19	0.43299	0.174296	0.134407	H41	0.54794	0.147305	0.366859	H62	0.160489	0.279567	0.625094
H20	0.40046	0.11435	0.101126	H42	0.61856	0.141313	0.339625	H63	0.30997	0.25919	0.348047
H21	−0.172941	0.00922422	0.860552	H43	−0.567011	0.114321	0.605416	H64	0.35657	0.318218	0.358447
H22	−0.160491	0.568184	0.787932								

[1] H. E. Lorenzana, I. F. Silvera, and K. A. Goettel, Phys. Rev. Lett. **64**, 1939 (1990).

[2] L. Cui, N. H. Chen, S. J. Jeon, and I. F. Silvera, Phys. Rev. Lett. **72**, 3048 (1994).

[3] F. Moshary, N. H. Chen, and I. F. Silvera, Phys. Rev. Lett. **71**, 3814 (1993).

[4] J. M. Leinaas and J. Myrheim, Nuovo Cimento B **37**, 1 (1977).

[5] J. V. Kranendonk, *Solid Hydrogen* (Plenum Press, New York, 1983).

[6] L. Cui, N. H. Chen, and I. F. Silvera, Phys. Rev. B **51**, 14987 (1995).

[7] R. J. Hemley, H. K. Mao, and J. F. Shu, Phys. Rev. Lett. **65**, 2670 (1990).

[8] A. F. Goncharov, J. H. Eggert, I. I. Mazin, R. J. Hemley, and Ho-kwang Mao, Phys. Rev. B **54**, R15590 (1996).

[9] Y. A. Freiman, S. M. Tretyak, A. Jezowski, and R. J. Hemley, J. Low Temp. Phys. **113**, 723 (1998).

[10] A. P. Brodyanskii, V. V. Sumarokov, Yu. A. Freiman, and A. Jezowski, Low Temp. Phys. **19**, 368 (1993).

[11] V. G. Manzhwlii and Y. A. Freiman, *Physics of Cryocrystals* (AIP Press, New York, 1997).

[12] B. Hetényi, S. Scandolo, and E. Tosatti, Phys. Rev. Lett. **94**, 125503 (2005).

[13] M. Trefler and H. P. Gush, Phys. Rev. Lett. **20**, 703 (1968).

[14] I. Pomeranchuk, Zh. Eksp. i Teor. Fiz. (USSR) **20**, 919 (1950).

[15] R. C. Richardson, Rev. Mod. Phys. **69**, 683 (1997).

[16] K. J. Runge, M. P. Surh, C. Mailhiot, and E. L. Pollock, Phys. Rev. Lett. **69**, 3527 (1992).

[17] M. P. Surh, K. J. Runge, T. W. Barbee III, E. L. Pollock, and C. Mailhiot, Phys. Rev. B **55**, 11330 (1997).

[18] T. Cui, E. Cheng, B. J. Alder, and K. B. Whaley, Phys. Rev. B **55**, 12253 (1997).

[19] H. Shin and Y. Kwon, J. Korean Phys. Soc. **54**, 1582 (2008).

[20] I. F. Silvera, Rev. Mod. Phys. **52**, 393 (1980).

[21] R. J. Hemley, H. K. Mao, L. W. Finger, A. P. Jephcoat, R. M. Hazen, and C. S. Zha, Phys. Rev. B **42**, 6458 (1990).

[22] I. F. Silvera and R. J. Wijngaarden, Phys. Rev. Lett. **47**, 39 (1981).

[23] I. F. Silvera, S. J. Jeon, and H. E. Lorenzana, Phys. Rev. B **46**, 5791 (1992).

[24] R. J. Hemley, J. H. Eggert, and H. K. Mao, Phys. Rev. B **48**, 5779 (1993).

[25] A. F. Goncharov, J. H. Eggert, I. I. Mazin, R. J. Hemley, and H. K. Mao, Phys. Rev. B **54**, R15590 (1996).

[26] I. Goncharenko and P. Loubeyre, Nature (London) **435**, 1206 (2005).

[27] H. M. James, Phys. Rev. **167**, 862 (1968).

[28] J. Kohanoff, S. Scandolo, G. L. Chiarotti, and E. Tosatti, Phys. Rev. Lett. **78**, 2783 (1997).

[29] H. Kitamura, S. Tsuneyuki, T. Ogitsu, and T. Miyake, Nature (London) **404**, 259 (2000).

[30] C. J. Pickard and R. J. Needs, Nat. Phys. **3**, 473 (2007).

[31] H. Miyagi and T. Nakamura, Prog. Theor. Phys. **37**, 641 (1967).

[32] H. Nagara and T. Nakamura, Phys. Rev. Lett. **68**, 2468 (1992).

[33] A. Laio and F. L. Gervasio, Rep. Prog. Phys. **71**, 126601 (2008).

[34] Y. Crespo, A. Laio, G. E. Santoro, and E. Tosatti, Phys. Rev. E **80**, 015702 (2009).

[35] J. Schaefer and W. E. Köhler, Z. Phys. D **13**, 217 (1989).

[36] P. G. Burton and U. E. Sneff, J. Chem. Phys. **76**, 6073 (1982).

[37] L. Monchick and J. Schaefer, J. Chem. Phys. **73**, 6153 (1980).

[38] P. Diep and J. K. Johnson, J. Chem. Phys. **112**, 4465 (2000).

[39] P. Wind and I. Roeggen, Chem. Phys. **167**, 263 (1992).

[40] P. Vinet, J. Ferrante, J. H. Rose, and J. R. Smith, J. Phys. C **20**, L467 (1986).

[41] D. M. Ceperley, Rev. Mod. Phys. **67**, 279 (1995).

[42] M. P. Allen and D. J. Tildesley, *Computer Simulation of Liquids* (Clarendon Press, Oxford, 1987).

[43] A. Chijioke and I. F. Silvera, Phys. Rev. Lett. **97**, 255701 (2006).

[44] M. A. Strzhemechny, Czech. J. Phys. **46**, 523, Suppl. S1 (1996).

[45] D. Frenkel, Physica A **263**, 26 (1999).